EFFECTS OF GLOBAL TARGET SHAPE ON IMPACT CRATERING, C. J. Byrne, Image Again, charles.byrne@verizon.net

Introduction: The impact cratering process is affected by two aspects of the shape of the target surface: a shape that conforms to the overall geoid and one that varies locally from the geoid. This paper considers the global shape of a spherical target. Two effects are analyzed: the elliptical trajectories of the ejecta (in the absence of an atmosphere) and the variation of depth of the deposited ejecta due to the spherical target.

The determination of the shape of the ejecta depth depends on the radial profile of ejecta velocity. A scalable velocity profile for lunar basins, partly physical and partly empirical, is presented.

Assumptions: The target and its geode are assumed to be approximately spherical and co-centric. The impactor is assumed to arrive at a high angle from the horizontal, so that the impact has nearly circular symmetry. Any atmosphere present in the target is assumed to be negligible, in respect to the size of the impact. The scaling laws for the gravity domain [1] are assumed valid with the radius being measured along an arc of the target surface, following the target's geoid.

Model of impact feature's ejection cavity: The model and scaling rules are taken from reference [1]. An ejection cone is produced at a constant angle φ with the horizontal and a magnitude of velocity $v\ (r)$, from $r = 0$ to the surface intercept radius. The surface intercept radius is at the intercept between the ejection cavity and the estimated target surface, at the inner base of the rim, and is taken to be equivalent to the term "radius of the transient cavity" in [1]. The distinction is made because there has been controversy about whether the radius of the physical transient cavity is greater or smaller than the radius of the excavation cavity.

The volume thrown from an incremental ejection ring per unit of radius is assumed to follow the scaling law [1] out to the surface intercept radius.

Calculation of the deposited depth: The incremental ejecta is thrown from the internal radius r to the deposit radius d = r + R, where R is the range of ejection (see Figure 1). The depth of the ejection field can be found by dividing the incremental volume of ejecta by the ratio of the area of the incremental deposit ring to that of the incremental ejection ring. The relative width of the rings is the derivative of R(r). The circumference of the rings depends on R, as will be described. An allowance may be made for an increase in porosity.

Elliptical trajectory: The equation for the range of an elliptical trajectory (see Figure 1) is [2], [3]:

$$R = 2R_t \tan^{-1}((v^2 / R_t g)\sin\phi\cos\phi /(1-(v^2 / R_t g)\cos^2\varphi))$$

Where g is the acceleration of gravity at the surface of the target, R_t is the radius of the target, and R is measured along an arc on the target surface. Ejecta from an incremental ring ejected at r is deposited at $d = r + R$.

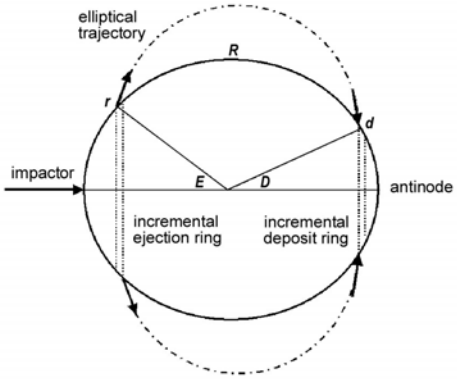

Figure 1: Deposit of ejecta from a large basin on a spherical target. R is the range of ejecta thrown out from the incremental ring at r and deposited at d. Radiii r and d are measured along arcs of the surface from the point of impact.

Spherical target: On a spherical target the circumference of each incremental ring depends on its radius, measured along the normal to the line between the point of impact and the antinode (see figure 1). The ratio of the circumference of the deposit ring to that of the ejection ring (a factor in the determination of ejecta depth) is the Sin(E)/Sin(D) (see Figure 1). The depth of the ejecta increases as it falls closer to the antinode until it becomes theoretically infinite there, where D = 0. Then it decreases again. In a real case, the chaotic nature of the ejection cone may diffuse the deposit at the antinode, the ejecta that is focussed at a point lands with a large horizontal component of velocity in all directions, and the dynamic angle of repose affects the way the ejecta settles.

For moderate-sized basins, the antinode is in the far field of the ejecta, but in the Near Side Megabasin [5], [8] it lies within the ejecta blanket. Therefore, a very large amount of ejecta gathers there.

Ejection velocity: The profile of ejection velociy as a function of the ejection radius is needed to carry out

the range calculations. The scaling laws provide for an exponentially decreasing function of r, but as the rim is approached, this must be modified to bring the ejection velocity to 0. An empirical curve was found that provides a good fit to the ejecta fields of 50 large craters and basins on the Moon (see Fgure 2). An energy-balance equation for the dependence of the magnitude of ejection velocity as a function of the radius [4] provides a good fit to the empirical profile, out to within 7º of the rim.

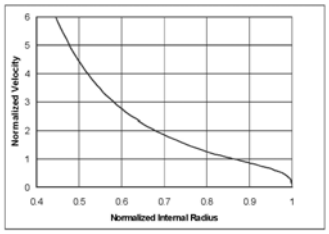

Figure 2: Ejection velocity as a function of radius.

Using a flat-surface target model, this equation, modified by an empirical segment near the rim, provided a scalable [1] radial profile of the ejecta field that was a good match to the radial profiles of 50 large craters and basins of the Moon.

Applications: Using the methods presented above, models of the lunar South Pole-Aitken Basin and the newly identified Near Side Megabasin [5] were produced (Figures 3 and 4).

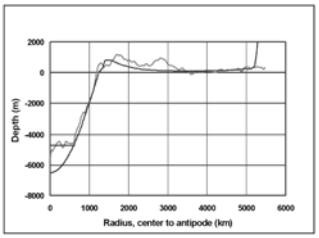

Figure 3: Model (after isostasy) and topographic radial profile of the South Pole-Aitken Basin

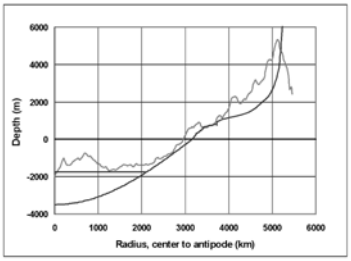

Figure 4: Model (after isostasy) and radial topographic profile of the Near Side Megabasin.

The model of these two giant basins, together with those of the other 50 large craters and basins mentioned above, explain many features of the Moon. In particular, both the topography [6] and crustal thickness [7] data are in good agreement with the model [8], [9] (Figure 5). To reconcile the topographic and crustal thickness data, full isostatic compensation is assumed for the South Pole-Aitken and the Near Side Megabasin.

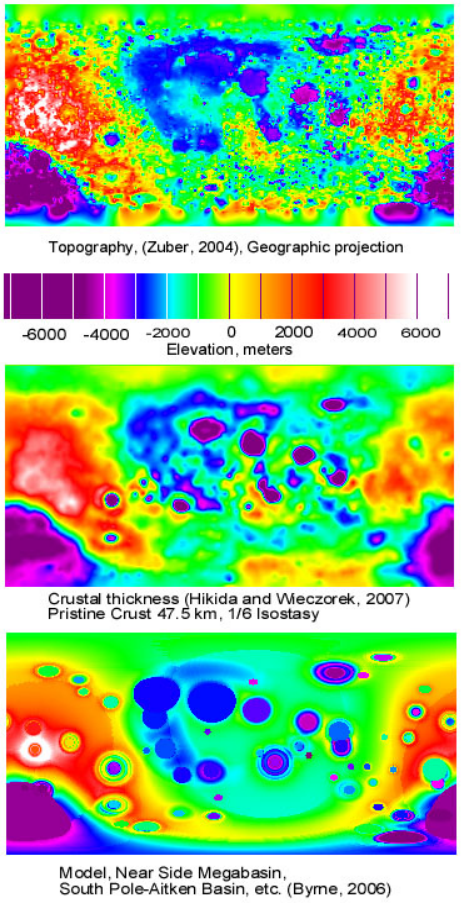

Figure 5: A comparison of the composite model with the current topography and the topography implied by crustal thickness data, after isostatic compensation.

References: [1] Housen, K. R., Scmidt, R. M., and Holsapple, K. A. (1983) JGR, Vol. 88, B3. [2] Melosh, H. J. (1989) Oxford University Press, 1989. [3] Ahrens and O'Keefe, (1976), LPSC VII. [4] Richardson, J. E. (2007), LPSC XXXVIII. [5] Byrne, C. .J. (2006), LPSC XXXVII. [6] Zuber, M. T., Smith, D. E., and Neumann, G. A. (2004), http//wufs.wustl.edu/geodata/clem1-gravity-topo-v1/. [7] Hikida, S. H. and Wieczorek, M. A., (2007), LPSC XXXVIII. [8] Byrne, C. J. (2007), A Large Basin on the Near Side of the Moon, paper submitted to Earth, Moon, and Science. [9] Byrne, C. J. (2007), The Far Side of the Moon, book submitted to Springer.